Exporting metal-carbene chemistry to live mammalian cells: Cop-per-catalyzed intracellular synthesis of quinoxalines enabled by N-H carbene insertions

Sara Gutiérrez
CIQUS, Universidade de Santiago de Compostela https://orcid.org/0000-0003-1257-4004
María Tomás-Gamasa
CIQUS, Universidade de Santiago de Compostela https://orcid.org/0000-0001-8681-2744
Jose Mascareñas (joseluis.mascarenas@usc.es)
CIQUS, Universidade de Santiago de Compostela https://orcid.org/0000-0002-7789-700X

Article

Keywords: bioorthogonal chemistry, diazocompounds, metal carbenes, copper, metal catalysis, intracellular chemistry

Posted Date: April 14th, 2021

DOI: https://doi.org/10.21203/rs.3.rs-331419/v1

Exporting metal-carbene chemistry to live mammalian cells: Copper-catalyzed intracellular synthesis of quinoxalines enabled by N-H carbene insertions

Sara Gutiérrez, María Tomás-Gamasa* and José L. Mascareñas*

Centro Singular de Investigación en Química Biolóxica e Materiais Moleculares (CIQUS), and Departamento de Química Orgánica. Universidade de Santiago de Compostela, 15782 Santiago de Compostela, Spain.

KEYWORDS. bioorthogonal chemistry, diazocompounds, metal carbenes, copper, metal catalysis, intracellular chemistry

Harnessing the power of transition metal catalysis in biological settings, and especially inside living cells, can open a world of new opportunities in chemical and cell biology, as well as in biomedicine. Yet, advancing in this endeavor requires to address major challenges associated to biocompatibility, transport and bioorthogonality issues, as well as the stability of the catalyst in these aqueous, crowded environments. This is especially relevant in reactions that involve the formation of organometallic intermediates that are considered labile, such as metal carbenes. Here, we demonstrate the viability of performing catalytic metal carbene intermolecular transfer reactions inside live mammalian cells. In particular, we show that copper (II) catalysts can promote the intracellular annulation of alpha-keto diazocarbenes with *ortho*-amino arylamines, in a process that is initiated by the insertion of the carbene into the N-H bond of the substrate. The potential of this transformation is underscored by the intracellular synthesis of a product that alters mitochondrial functions, and by demonstrating cell selective biological

responses using targeted copper catalysts. Considering the wide reactivity spectrum of metal carbenes, this work opens the door for significantly expanding the repertoire of reactions that can be performed in live environments and for unveiling new biological applications.

Live cells can be viewed as microfactories that perform thousands of simultaneous chemical reactions in a highly regulated manner. Most of these reactions are promoted by enzymes, proteins that have evolved to exhibit exquisite rates and selectivities.[1-2] Over one-third of the enzymes feature metals at their active sites, and therefore are coined as metalloenzymes. In recent years, there has been an impressive progress in the creation of laboratory versions of metalloenzymes that catalyze "new-to-nature" reactions.[3-9] However, the application of these catalytic metalloproteins has been essentially restricted to the realm of synthetic methodology. Their use for biological purposes, in the natural environments of enzymes (living cells or organisms), is more challenging, and remains to be uncovered.[10-13]

An alternative approach to perform artificial chemical reactions in live cells has recently emerged, and consists of the use of exogenous, discrete transition metal catalysts.[14-19] While the catalytic activity of these reagents is far away from that of metalloenzymes, they can permeate living cells, and eventually trigger non-native organometallic reactions. Therefore, several transition-metal reagents that mediate intracellular allylic or propargylic deprotections,[20-27] cyclizations,[28-29] cross couplings,[30-33] or even formal cycloadditions,[34-38] have been recently disclosed. However, the portfolio of reactions is yet too small, especially when compared with the enormous breadth and potential that organometallic catalysts exhibit in organic solvents.

A particularly powerful class of organometallic reagents that have been widely used in synthesis, but not yet applied in biorthogonal and intracellular catalysis, are discrete metal carbenes.[39] This might be in part due to the notion that these intermediates, and even their diazo precursors, are too fragile and reactive, and might not survive in water, and especially to the presence of native biomolecules with reactive nucleophilic functionalities like amines or thiols (Fig. 1a, left). However, some isolated examples suggest

that diazocompounds can be used for bioorthogonal tagging.[40-42] Moreover, several chemoselective functionalizations of peptides and proteins relying on C-H activations promoted by rhodium carbenes have been reported.[43-47] Gillingham and coworkers have also described DNA modification reactions using rhodium or copper (I) carbenes capable of inserting into the N-H bond of adenines.[48-49]

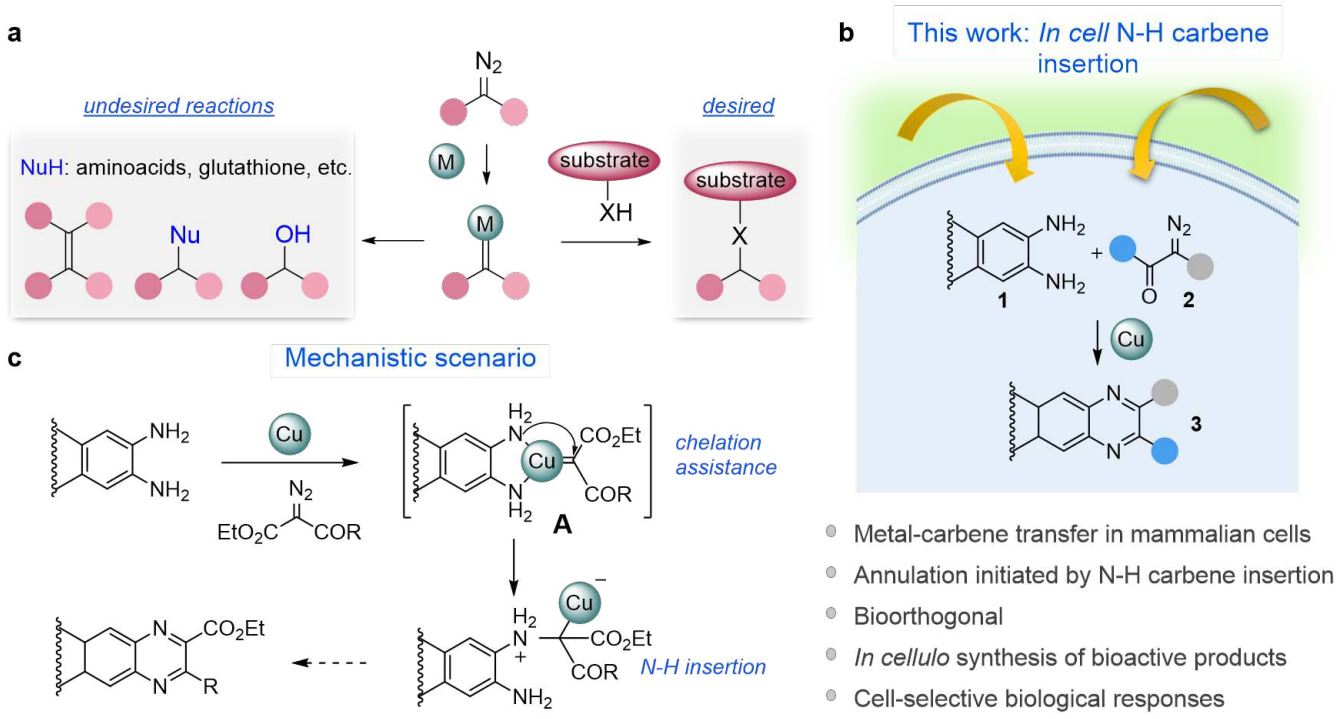

Figure 1. Metal N-H carbene insertions in biological settings. a, Orthogonality challenges in metal-mediated carbene transfer transformations in aqueous/biological media. **b**, Copper-promoted annulation initiated by an N-H carbene insertion within biological and/or cellular environments. **c**, Mechanistic outline: The copper carbene sticks to the diamine owing to the bidentate coordination. This might favor the N-H insertion, which is followed by an intramolecular condensation and oxidative aromatization.

In addition to these examples, metallocarbene transfer reactions have been developed in the context of artificial metalloenzymes, using heme-containing proteins expressed in *E. Coli* strains, especially with native iron cofactors,[50-58] though these advances can be ascribed to the fields of synthetic methodology and synthetic biology.[59-61]

In this context, we questioned whether it would be possible to perform metal-catalyzed carbene transfer reactions in biorelevant aqueous mixtures and eventually in live mammalian cells (Fig. 1). Adding this

type of catalytic reactions to the catalog of life-compatible organometallic processes might foster unprecedented opportunities for cellular and biological intervention given the power and versatility of metal-carbene chemistry. However, this goal raises many challenges and questions: Will diazo reagents be able to capture the metal complex in a challenging biological milieu to generate the metal carbenes? Are these metal-carbene intermediates compatible with biological molecules and stable enough to react with designed reactants? Can we perform this chemistry within living cells? Can we use these reactions to build abiotic bioactive products in cells, and elicit biological effects?

Herein we report a successful realization of these goals, by disclosing the first metal-catalyzed carbene transfer reaction carried out in the interior of living mammalian cells. The reaction has been implemented with *ortho*-amino arylamines, providing for the assembly of photophysically and/or biologically relevant quinoxaline products (Fig. 1b). The transformation likely benefits from a chelation assistance process to generate intermediates like **A**, which favors the N-H insertion, initial step of the process (Fig. 1c). We also demonstrate that this technology can be used for the *in cellulo* synthesis of a compound that promotes mitochondrial fragmentation and depolarization, and produces cytotoxic effects. Importantly, by equipping the copper ligand with suitable targeting units, it is possible to elicit cell selective responses.

Results and discussion

Finding the right catalyst. At the outset, we needed to identify a suitable reaction involving a metal-carbene transfer process that could be easily monitored, eventually, by fluorescence microscopy. In this context, we were attracted by the annulation between 1,2-diaminobenzenes and α-diazo-β-keto esters, which was described to work in water at 70 °C, using $Fe(OTf)_3$ as catalyst, and involves as initial step an N-H insertion of the iron carbene.[62] In particular, we selected the reaction of 2,3-diaminonaphthalene (**1**) which can provide fluorescent benzoquinoxalines such as **3a** (Fig. 2a). We reasoned that the second amine group in the substrate could play a very important role not only to drive the generation of cyclic products, but also as metal coordination handle to enhance reactivity and favor orthogonality in the presence of competing nucleophiles (Fig. 1c).[63-64]

We began our work by exploring the reaction between diamine **1** and 2-diazo-3-oxo-3-phenylpropanoate (**2a**) in water (Fig. 2a), in presence of different transition metal catalysts, including the previously described $Fe(OTf)_3$. Unfortunately, treatment of diamine **1** with 1 equiv. of diazocarbonyl **2a** and 10 mol% of $Fe(OTf)_3$ in water (100 mM) at 40 °C for 24 h led to no conversion. Other iron (III) catalysts ($FeCl_3$, $Fe(acac)_3$) were also ineffective.

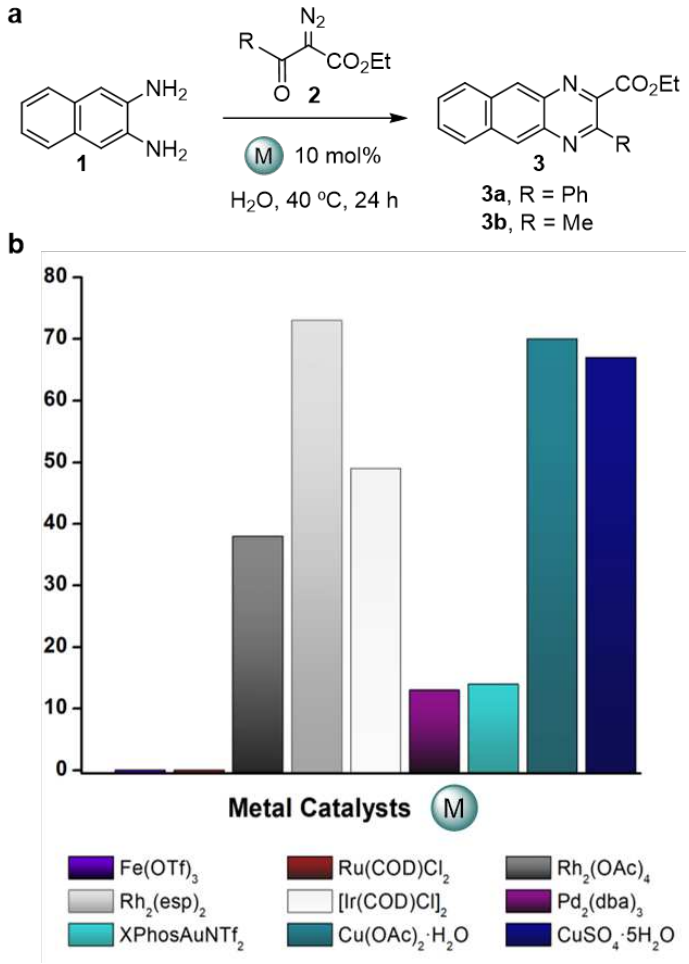

Figure 2. Metal-catalyzed assembly of quinoxalines in water. **a**, Annulation reaction. **b**, Screening of different transition metal catalysts. [a] Reaction conditions: 1 equiv. **1** and **2**, in H_2O (100 mM), in presence of 10 mol% catalyst, and heating of the resulting heterogeneous mixture at 40 °C for 24 h. Yield calculated by ^{1}H-NMR using 1,3,5-trimethoxybenzene as internal standard.

We then made a screening using several transition metal complexes that were previously used in N-H carbene insertion reactions (Fig. 2b).[65] $Ru(PPh_3)_3Cl_2$, $Ru(COD)Cl_2$, $RuCl_3{\cdot}H_2O$, AgOTf, $CoCl_2$ and $Co(OAc)_2{\cdot}4H_2O$ failed to give any product, and using gold or palladium reagents like $XPhosAuNTf_2$,

$Pd_2(dba)_3$ we observed testimonial amounts of the desired adduct **3a** (13-18%). Rhodium or iridium catalysts like $[Rh_2(OAc)_4]$, $[Rh(COD)Cl]_2$, $[Cp^*IrCl_2]_2$, $[Ir(COD)Cl]_2$ and $[Ir(COD)(OMe)]_2$ did promote the reaction at room temperature, but in modest yields (100 mM, 20-49% yields). With $Rh_2(esp)_2$ the reaction was more efficient (72% yield); however, under more diluted conditions, the reaction gave an undesired side product resulting from addition of water to the carbene (**4**, $CO_2EtCH(OH)COPh$, 50% yield). Fortunately, copper (II) salts were catalytically active and efficient, and in this case we didn't observe the formation of the water insertion product, but only small amounts of a carbene-derived dimer (**4'**). Control experiments in the absence of diamine **1** led to a mixture of the dimer **4'**, and the O-H insertion product **4** (Supplementary Fig. 1).

In view of these results, we next made an optimization study with the copper catalysts (Fig. 3a and Supplementary Tables 1-4). Different copper salts, either featuring Cu(I) or Cu(II), were effective, providing the desired azaheterocycle product in yields ranging from 56 to 70% (entries 1-4). Remarkably, the catalyst loading could be decreased to 5 mol% without affecting the yield (entry 5). Even using only 1 mol%, we observed more than 50% of the product (entry 6). The ratio of reactants doesn't seem to be crucial, since no relevant changes were observed by modifying it (entry 7). A pH 7 was found to be optimal, nonetheless carrying the reaction at acidic (below 4) or basic pH (9.5) led to only a slight decrease in the yield (over 60%, Supplementary Table 2). Other diazo reagents could also be used, and therefore product **3b** was formed in a good 67% yield after 24 h (57% isolated yield, entry 8). The use of cosolvents, such as acetonitrile, didn't bring special improvements in the efficiency of the process (Supplementary Table 3). The reaction can also be carried out under neat conditions leading to 59% yield (entry 9). Remarkably, using diluted conditions (5 mM) the reaction was more efficient (93% yield after 24 h, entry 10), likely due to the suppression of the side dimerization reaction.

a

Entry	Catalyst	Deviation from standard conditions[a]	% Yield (3a)
1	$Cu(OAc)_2 \cdot H_2O$	-	70
2	$Cu(OTf)_2$	-	56
3	$[(MeCN)_4Cu](OTf)$	-	64
4	$[(MeCN)_4Cu]PF_6$	-	62
5	-	5 mol% [Cu]	72 / 66[b]
6	-	1 mol% [Cu]	53
7	-	5 mol% [Cu] 1.5 equiv diamine	75
8	-	**2b**	67 / 57[b] (**3b**)
9	-	neat	59
10	-	5 mM	93

b

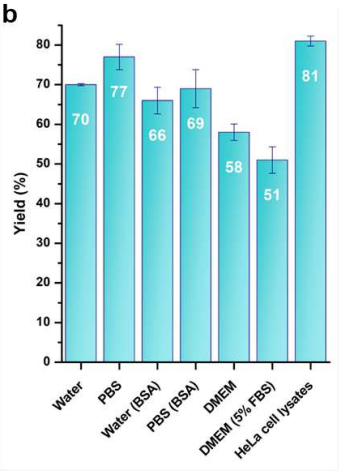

c

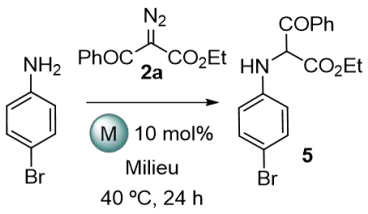

Milieu	% Yield (**5**) $Cu(OAc)_2$	% Yield (**5**) $[Ir(COD)Cl]_2$
H_2O	33	74
PBS	34	66
cell lysates	—	64

Figure 3. Copper-carbene mediated synthesis of quinoxalines 3. a, Further optimization of the reaction between **1** and **2a** or **2b**. **b**, Efficiency in presence of biological buffers. BSA 5 mg/mL; Cell lysates 4 mg/mL (the values are average of three experiments, and error bars correspond to standard deviations). **c**, Monoaminations by N-H insertion. [a] Reaction conditions: H_2O as solvent, 100 mM, 10 mol% catalyst, 40 °C, 24 h; [Cu] = $Cu(OAc)_2$. Yield calculated by ^{1}H-NMR using 1,3,5-trimethoxybenzene as internal standard. [b] Isolated yield.

Bioorthogonality. As the goal was moving to biological media, it was key to uncover the tolerance of the reaction to the presence of biological additives and salts. We were glad to observe that in saline phosphate buffer (PBS, pH = 7.2, 100 mM) the reaction was slightly more efficient than in water (77% yield using 10 mol% of the catalyst, Fig. 3b). Unfortunately, in this case further dilution negatively affected the yield. Good results were also observed when the reaction was carried out in the presence of biological additives like BSA (bovine serum albumin, 5 mg/mL), a protein that features one free cysteine and several histidines in its structure. Importantly, the transformation tolerates more stringent conditions such as cell culture media like DMEM (Dulbecco's modified Eagle's medium), that contains many additives (vitamins, amino acids, etc.), although it was slightly less efficient (58% yield). Even in DMEM containing 5% of FBS (fetal bovine serum) the reaction takes place, providing a 51% yield of the product. Finally, the process is also compatible with HeLa cell lysates (4.0 mg/mL); indeed, this milieu was even benefitial for the efficiency of the reaction (81% after 24 h). Using lower catalyst loadings (5 mol%) the

product is obtained in a satisfactory 73% yield, but at lower concentrations (25 mM) the yield decreased to 63% (Supplementary Table 5).

The reaction yield in water (100 mM) was not affected by the presence of 10 mol% (1 equiv. with respect to the copper complex) of different types of amino acids, like glycine or valine, glutamic acid, lysine, histidine or tyrosine, and even of cysteine or methionine. The reaction also tolerates the presence of larger amounts (1 equiv. with respect to the susbtrate) of amino acids like tyrosine or lysine, carbohydrates such as glucose, nitrogenous bases such as guanine or cytosine or reductant agents such as sodium ascorbate, providing yields between 50-62% of the product. However, it is inhibited by additives featuring nucleophilic heteroatoms, like adenine or glutathione, very likely because these compounds coordinate to the copper catalyst producing inactive off-cycle complexes. Curiously, when the same reaction was performed in PBS instead of water, even in presence of 10 mol% of glutathione, the product was formed in a 66% yield. This result suggests that saline media like PBS might somewhat disfavor the irreversible formation of inactive copper complexes (Supplementary Fig. 2).

Other N-H insertions. The above annulation reaction can be considered as a tandem process that involves three steps: the key N-H carbene insertion, an intramolecular amine-carbonyl condensation, and a final oxidative aromatization (Fig. 1c). A pertinent question is related to the viability of achieving similar catalytic reactions that only involve the N-H insertion process. Preliminary experiments using 4-bromoaniline and diazo **2a** in water or PBS, with $Cu(OAc)_2$ (10 mol%, 40 °C, 24 h, 100 mM), revealed the formation of the desired N-H insertion product **5**, albeit with modest yield (33 and 34%, respectively, Fig. 3c). The reaction with $[Ir(COD)Cl]_2$[65] was cleaner and afforded the desired product in a satisfactory 74% yield in water. The efficiency of this catalyst did not diminish when changing the solvent to PBS (66% yield) and even in the presence of HeLa cell lysates (4.0 mg/mL, 64% yield). In fact, under this latter conditions, $Cu(OAc)_2$ failed to give the insertion product. These results point towards $[Ir(COD)Cl]_2$ as a promising catalyst for future studies in bioorthogonal metal-carbene insertions.

At this point we also wondered about the chemoselectivity of the parent Cu-promoted annulation of 2,3-diaminonaphthalene (**1**), in presence of equivalent amounts of competing monoamines

(Supplementary Table 6). We observed that the reaction yield was not affected by the presence of aromatic amines, such as 2-naphthylamine, aniline or 4-bromoaniline, as well as by the addition of phenol. This clear kinetic preference might be associated to the chelating effect of the neighbour amino group (Fig. 1c, **A**). In consonance, the presence of strong chelating diamines decreased the yield (with ethylenediamine, 40%), or completely inhibited the reaction (with 2-picolylamine, 8-aminoquinoline).

Catalytic reactivity in mammalian cells. The stage was set to move to a more complex, real life scenario, such as that of mammalian cells. Note that a cell medium cannot be fully equated to the above *in vitro* conditions, and might be better viewed as an aqueous, crowded gel. Fluorescence spectroscopy confirmed that whereas the diamine substrate **1** presents a very low emission above 500 nm when excited at 385 nm, the product **3a** displays high fluorescence (Supplementary Fig. 3,4). These emission properties were also confirmed in living cells: incubation of HeLa cells with **3a** (100 μM), DMEM washing, and observation under the microscope, revealed a clear intracellular emission (Fig. 4a, panel B), not observed for **1** and **2a** (panel A). For the intracellular reactions, HeLa cells were incubated with $Cu(OAc)_2$ for 50 min (50 μM) in DMEM, washed to remove extracellular copper salts (2xDMEM), and treated with the substrates (**1** and **2a**, 100 μM each). Observation under the fluorescence microscope after 1.5 h revealed an intracellular buildup of green fluorescence in the cytosol, which must be associated to the formation of product **3a** (Fig. 4a, panel C). Monitoring the process with time confirmed a progressive increase in intensity, in consonance with the intracellular generation of more product (Fig. 4a, panel D and Supplementary Fig. 8). Control experiments of cells treated with the copper complex or with only one of the components, either **1** or diazo **2a**, led to essentially no fluorescence (Supplementary Fig. 9). Similar results were obtained using MCF7 cells (Fig. 4a, panel E,F).

Morphological analysis of the cells after the reaction time was indicative of a reasonably good status in terms of viability, which was confirmed using standard MTT tests. As detailed in the Supplementary Note 9, the Cu(II) salt didn't compromise the cell viability, even after 12 h. Similarly, neither **1**, **2a** nor product **3a** affected the viability of the cells (complete survival after 18 h). Very importantly, the intracellular formation of product **3a** was further confirmed by mass spectrometry, after extraction of the cell contents

with MeOH (Fig. 4b). Indeed, using this protocol (Supplementary Note 13) we could even quantify the product, which combined with the amount of intracellular copper calculated using ICP analysis allowed to estimate a TON of over 7 (incubation time of 5 h, Fig. 4b, average of several experiments, Supplementary Note 12 and 13).

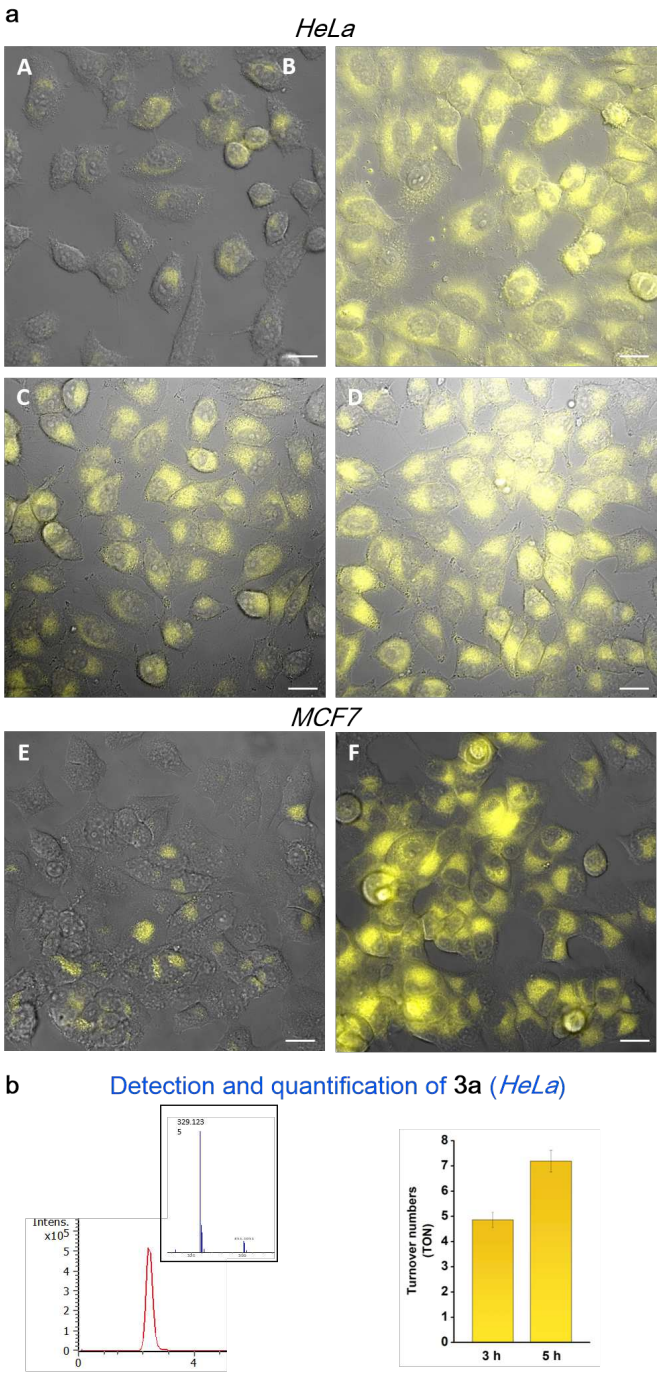

Figure 4. Synthesis of 3a inside live HeLa cells. a, Fluorescence micrographies (brightfield) of HeLa (A-D) and MCF7 cells (E,F) after incubation with: **1** and **2a** (A, E); **3a** (B) or $Cu(OAc)_2$, washing, and treatment with **1** and **2a** for 1.5 h (C) or for 3 h (D,F). Reactions conditions: Cells were pretreated with 50 μM of $Cu(OAc)_2$ (stock solution in H_2O) for 50 min, washed twice with DMEM, and incubated with 100 μM of substrates **1** and **2a** (stock solutions in DMEM) for the indicated time. **b**, Detection and quantification of **3a** in HeLa cells. *Left*: Extracted ion chromatogram of the product (**3a**) generated intracellularly (methanolic extract); *Right*: Quantification of turnover numbers (average of three experiments), considering the product present in the cell media and washes (2xDMEM, 1xPBS) and in the methanolic cellular extracts (over 75% of the total). Scale bar: 20 μm. λ_{exc} = 385 nm, λ_{em} > 520 nm.

Eliciting biological effects. Developing *in cellulo* metal-promoted transformations, and specifically metal carbene transfer reactions, is itself relevant from a fundamental perspective. However, a major challenge in the area is the demonstration that the reactions can find biological or biomedical applications. Indeed, several metal-promoted uncaging reactions have already been used to activate proteins or release bioactive agents.[66] However, "anabolic" processes, based on bond-forming reactions to build bioactive products, are much less developed.[67-70] Quinoxaline scaffolds are found in many biorelevant compounds, and therefore, we questioned whether our technology could enable the synthesis of bioactive quinoxalines inside live cells. In this context, we were called by Tyrphostins (TYRosin PHOSphorylation INhibitors),[71-72] compounds that exhibit a variety of interesting biological profiles, apparently as a consequence of their tyrosine kinase inhibitory activity. Remarkably, whereas **3a** was rather innocuous to cells (Supplementary Fig. 7), benzoquinoxaline **3c**, also called Tyrphostin AG1385,[73] promoted a decrease in the cell viability of 40% after 12 h (50 μM). Noteworthy, using higher concentrations (100 μM) we didn't observe a further increase in the cell death (Fig. 5b), a result that can be explained because of the tendency of this highly hydrophobic product to aggregate and precipitate, which compromises its internalization. In consonance with the previous results, product **3c** can be readily made applying our carbene transfer methodology using reactants **1** and diazo compound **2c** (Fig. 5a and Supplementary Note 5 for its *in vitro*

synthesis). Therefore, after addition of 50 μM of the reactants (**1** and **2c**) to HeLa cells previously treated with $Cu(OAc)_2$ (25 μM), we observed a similar effect in the cell viability than by direct incubation with **3c**. More relevant, using higher concentrations of the substrates (up to 100 μM) the effect on cell survival is higher (less than 30% of cell viability, Fig. 5b). These results underscore one of the potential advantages of generating bioactive products by intracellular synthesis versus their external addition. Product **3c** presents low levels of fluorescence, which precludes its detection under the microscope; however, we could confirm and quantify its intracellular formation by MS of cellular extracts obtained after carrying out the cellular reaction (after 4.5 h we calculated TONs over 4, Supplementary Note 13).

Given that some tyrphostins have been shown to affect mitochondria,[73] we tested whether the intracellular generation of **3c** could affect the mitochondrial membrane potential, a property that can be monitored by measuring the fading of TMRE (tetramethyl rhodamine methyl ester) staining. Depolarized or inactive mitochondria have decreased membrane potential and fail to sequester TMRE.[74] Gratifyingly, while treatment of HeLa cells with $Cu(OAc)_2$ and either substrate **1** or **2c** (100 μM) doesn't alter the mitochondria potential, after 3.5 h (Fig. 5c, panel A and Supplementary Fig. 10), addition of both reactants to cells previously treated with $Cu(OAc)_2$ (50 μM) led to a much more diffuse and less intense fluorescent signal of TMRE, indicating a depolarized mitochondria, which is in consonance with the *in situ* formation of **3c** (Fig. 5c, panel C). Indeed, direct addition of **3c** led to similar qualitative results (Fig. 5c, panel B). The same effect was observed with other type of cancer cell lines like MCF7 (differences in staining in panels D-F) and HEK293 (Supplementary Fig. 11). Remarkably, leaving the HeLa cells for a longer time (8 h) allows to recover, at least partially, the TMRE staining, however the mitochondria presented a different morphology, consistent with a considerable fragmentation (Figure 5d, panels G,I,K and Supplementary Fig. 12).

Using MitoTracker Green as mitochondrial dye, whose staining ability is less dependent on the polarization state of the organelles, we could confirm the fragmentation effect associated to the generation of **3c**. Cells treated only with substrates displayed a very well-defined network of tubular mitochondria, pre-

dominantly in fusion state (Fig. 5d, panel H). However, addition of **3c** (100 μM) resulted in more fragmented mitochondria (Fig. 5d, panel J). More importantly, a similar fragmented network, which is associated to fission, was also observed by generating the compound *in situ*, using our copper catalyzed transformation (Fig. 5d, panel L and Supplementary Fig. 13).

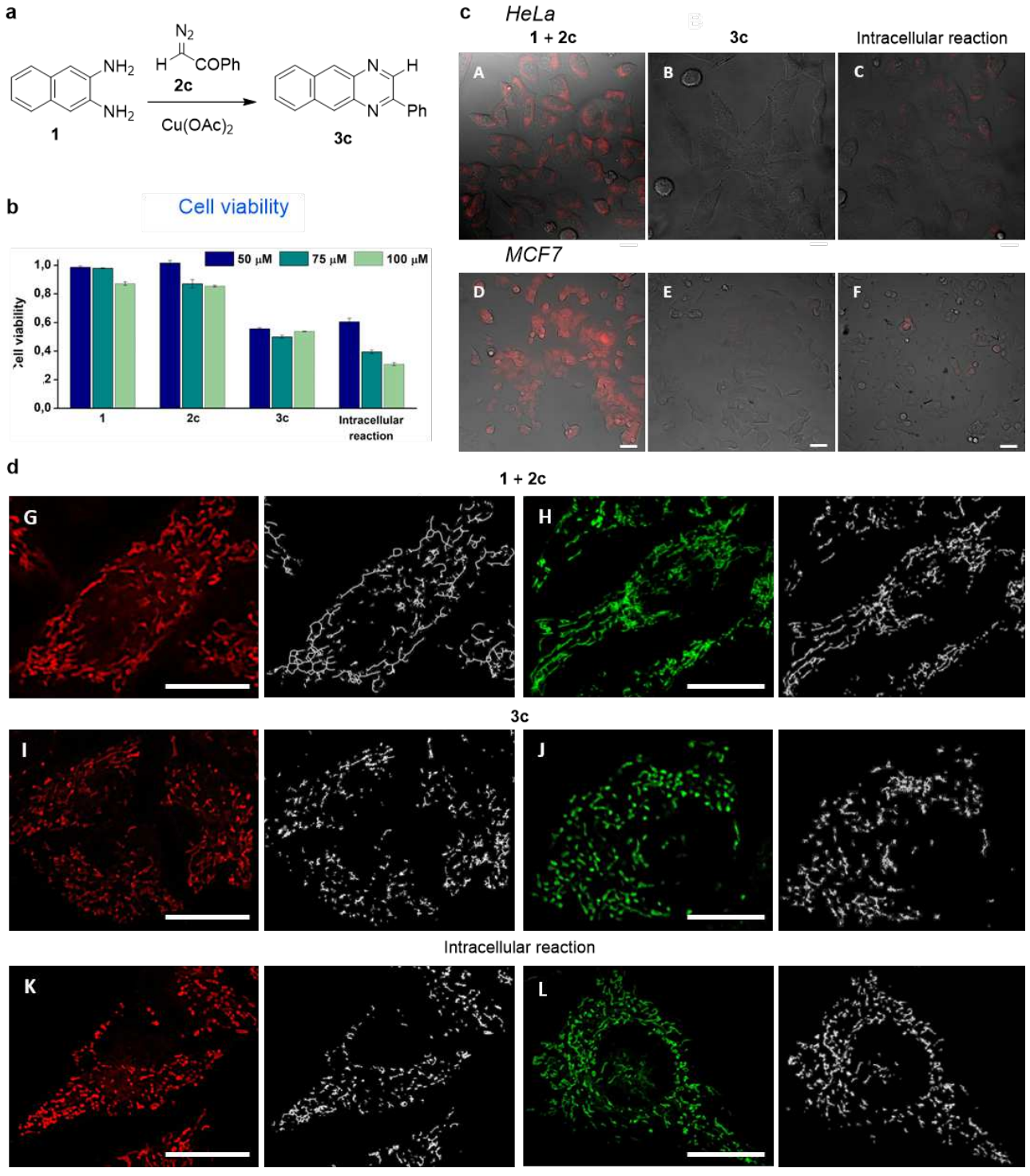

Figure 5. Intracellular generation of 3c. a, Synthesis of **3c**. **b**, Cytotoxicity studies. HeLa cells were mixed with either **1** and **2c**, or **3c** (50-100 μM) for 12 h; for the intracellular reaction cells were incubated with $Cu(OAc)_2$ (25-50 μM) for 50 min, washed twice with DMEM and treated with substrates **1** and **2c** (50-100 μM) for 12 h. **c**, Mitochondrial depolarization. Fluorescence micrographies using TMRE as marker: HeLa (A-C), and MCF7 cells (D-F) (brightfield) after incubation with: **1** and **2c** (A,D); **3c** (B,E); $Cu(OAc)_2$, washing, and treatment with **1** and **2c** (C,F) for 3.5 h. **d**, Mitochondrial fragmentation. Fluorescence micrographies of HeLa cells (brightfield) using TMRE (G,I,K) or MitoTracker Green (H,J,L) as marker, after incubation with: **1** and **2c** (G,H); **3c** (I,J) or $Cu(OAc)_2$, washing and treatment with **1** and **2c** for 8 h (K) or 2 h (L); in white, mitochondrial staining from each image displayed as a skeleton network using the ImageJ skeleton filter, which allows a better visualization of the fragmentation. Reaction conditions: Cells were mixed with **1** and **2c**, or **3c**. For the intracellular reaction cells were incubated with $Cu(OAc)_2$ (50 μM) for 50 min, washed twice with DMEM and treated with substrates **1** and **2c** (100 μM) and incubated with TMRE or MitoTracker Green (100 nM) for 10 min. Scale bar: 20 μm (15 μm in section c). λ_{exc} = 550 nm, λ_{em} = 570-590 nm for panels A-K; λ_{exc} = 470 nm, λ_{em} = 490-580 nm for panels H-L.

Targeted catalysts and cellular selectivity. A major dream in pharmacology is related to the possibility of delivering or accumulating drugs in specific, desired cellular targets. Even more attractive is the prospect of a catalytic generation of drugs in a cell-selective manner. We evaluated this possibility by building the conjugate **6**, shown in Figure 6a, which features an integrin-targeting motif (RGD: Arg-Gly-Asp) linked to a copper triazolyl ligand (BTTAA, Supplementary Note 6).[36] Hypothetically, this tripeptide motif might favor the preferential targeting of cell lines expressing substantial amount of integrins, such as HeLa cancer cells.[75] The conjugate was also engineered to exhibit a rhodamine dye (TAMRA) linked to a lysine side chain, in order to monitor the cellular fate of the complex. The copper complex (**6-Cu**) was formed *in situ*, just before the addition to cells by treatment of hybrid **6** with $CuSO_4$ (0,5 eq) in water (10 min). The formation of **6-Cu** was confirmed by LC-MS (Supplementary Fig. 6).

As depicted in Figure 6a (panel A), addition of **6-Cu** (15 μM) to HeLa cells, and subsequent washing (2xDMEM), gave rise to a substantial intracellular staining. In contrast, using MCF7 or HEK293 cells, which are known to exhibit lower levels of integrin receptors, we observed much less fluorescence (Fig. 6a, panel B and Supplementary Fig. 14 for HEK293). Further analysis by CTCF (corrected total cell fluorescence) corroborated the better uptake of HeLa cells (Fig. 6a, right). More importantly, in consonance with this programmed internalization of the copper complex, we observed a much higher increase in the fluorescence associated to the formation of product **3a** in HeLa cells, after treatment with reactants **1** and **2a** (Fig. 6b, panels C and D, respectively and Supplementary Fig. 15). It is important to note that using $Cu(OAc)_2$ instead of **6-Cu**, MCF7 cells are also able to generate the product (Fig. 4), which confirms that the above cell selective responses are associated to the preferential targeting and internalization properties of our designed catalyst 6-**Cu**.

This cell-dependent reactivity was also observed in the reaction leading to the mitochondria active quinoxaline **3c**. Therefore, treatment of the cells with **6-Cu** (15 μM), washings (2xDMEM) and addition of **1** and **2c**, led, after 3.5 h, to a substantial mitochondrial depolarization only in HeLa cells (Fig. 6c, panel G). MCF7 and HEK293 cells remain essentially intact (Fig. 6c, panel J and Supplementary Fig. 16). Control experiments with product **3c** revealed a similar depolarization effect in all cell lines, independently of their integrin expression (Fig. 6b, panels F,I). Figure 6d represents a quantification of the resulting TMRE staining.

All these results confirm the viability of using transition-metal carbene transfer catalysts for a cell selective synthesis of bioactive products and set the bases for future biological and biomedical applications.

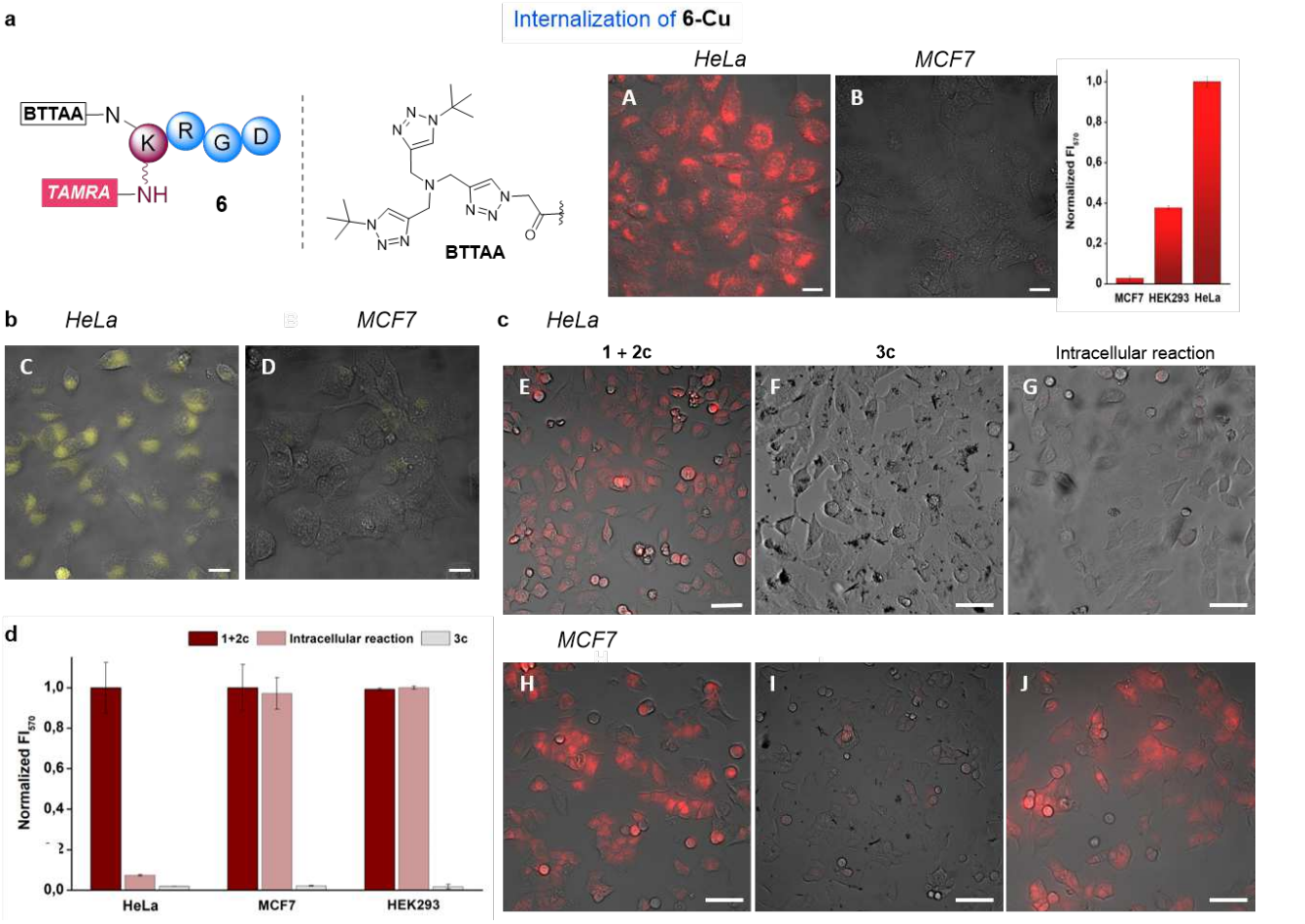

Figure 6. Selective cellular targeting using a RGD copper-containing peptide (6-Cu). a, Structure of the RGD containing ligand in **6-Cu**; Comparison of internalization of **6-Cu**. Fluorescence micrographies of HeLa (A) and MCF7 cells (B) (brightfield) and CTCF measurements in HeLa, MCF7 and HEK293 cells. Conditions: cells were incubated with 15 µM of **6-Cu** for 1.5 h. **b**, Fluorescence micrographies of HeLa (C) and MCF7 cells (D) (brightfield) after incubation with **6-Cu**, washing, and treatment with **1** and **2a** for 3.5 h. Scale bar: 20 µm. **c**, Cell-selective mitochondrial depolarization: Fluorescence micrographies of HeLa (E-G) and MCF7 cells (H-J) (brightfield) after incubation with: **1** and **2c** (E,H), product **3c** (F,I), or **6-Cu**, washing, and treatment with **1** and **2c** for 3.5 h (G, J). **d**, Bar graphic including CTCF measurements of mitochondrial depolarization in HeLa, MCF7 and HEK293 cells. Reaction conditions: cells were mixed with **6-Cu** (15 µM) for 1.5 h, washed twice with DMEM and treated with **1** and **2a**, or **1** and **2c** (100 µM) for 3.5 h followed by TMRE (100 nM) for 10 min. Scale bar: 100 µm. λ_{exc} = 550 nm, λ_{em} = 570-590 nm for panels (A,B,E-J); λ_{exc} = 385 nm, λ_{em} > 520 nm for panels (C,D).

Conclusions

We have described the first examples of a transition metal catalyzed carbene-transfer reaction inside living mammalian cells. The reaction entails a N-H insertion of a copper carbene into aromatic 1,2-diamines, and allows to generate benzoquinoxalines, owing to a subsequent intramolecular imine condensation and oxidative aromatization process. Therefore, the whole process, while capitalizing in the initial intermolecular carbene transfer reaction, entails two additional chemical steps. Preliminary studies confirmed the existence of a significative TON (of up to 7), which stresses the viability of performing catalytic carbene chemistry "in cells". Importantly, we have also developed initial examples that underscore the biological potential of the approach. The catalytic chemistry can be used for the intracellular synthesis of mitochondrial fragmenting agents, providing for more efficient biological responses than when using a direct addition of the bioactive products. Moreover, by conjugating the copper catalyst to an integrin targeting moiety, it is possible to achieve cell-selective biological effects.

The demonstration that metal-promoted reactions involving N-H carbene insertions can be carried out in the complex environment of a mammalian cell should foster further research to merge metal carbene catalysis and biological chemistry.

Methods

General

Chemical synthesis procedures, detailed protocols, and characterization of all the compounds are included in the Supplementary Information. For UV, fluorescence and NMR analysis of the compounds in this article, see Supplementary Notes 4 and 7.

Synthesis of compound **2a**: To a solution of *p*-acetamidobenzenesulfonyl azide (*p*-ABSA, 2.4 g, 10.0 mmol, 1.2 eq.) in dry acetonitrile (17.0 mL), at 0 °C under nitrogen was added ethyl benzoylacetate (1.8 mL, 8.3 mmol, 1.0 eq.). Then, DBU (1.5 mL, 10.0 mmol, 1.2 eq.) was added dropwise and the resulting red solution was stirred at 0 °C for 3 h, and slowly brought to room temperature. Upon completion as indicated by TLC, the reaction was quenched with water, extracted with ethyl acetate, dried and concentrated under reduced pressure. The residue was purified by silica flash column chromatography using hexane / EtOAc (9:1) as eluent to afford product **2a** as a yellow oil (1.8 g, 8.2 mmol, 99%).

Synthesis of compound **2c**: To a solution of benzoylacetone (649.0 mg, 4.0 mmol, 1.0 eq.) and *p*-ABSA (961.0 mg, 4.0 mmol, 1.0 eq.) in EtOH (4.0 mL) was added $MeNH_2$ (40% aqueous solution, 0.42 mL, 4.8 mmol, 1.2 eq.).. Upon addition of methylamine, an exothermic reaction was observed; the reaction mixture turned orange, then pale-yellow and finally became thick. To ensure an adequate stirring, 4.0 mL of

EtOH were added and the mixture was stirred at room temperature for 1 h. Upon completion of the reaction, as indicated by TLC, the mixture was concentrated under reduced pressure and the residue was purified by silica flash column chromatography using: hexane / EtOAc (9:1) as eluent to afford **2c** as a yellow solid (495.0 mg, 3.4 mmol, 85%).

Representative procedure for the catalytic reaction in water: To a 2.0 mL vial containing a stir bar and diazocarbonyl **2a** (21.8 mg, 0.1 mmol, 1.0 eq.), Milli-Q water (1.0 mL) was added, followed by 2,3-diaminonaphthalene **1** (15.8 mg, 0.1 mmol, 1.0 eq.) and the corresponding metal catalyst (10 mol%). The Thermowatch-controlled heating block was fixed at 40 °C and the heterogeneous reaction mixture was stirred for 24 h, open to air. Then, the mixture was transferred to a separating funnel and extracted with ethyl acetate (3 x 3.0 mL). The combined organic fractions were dried, filtered, concentrated and analyzed by ^{1}H-NMR. The yield was determined by ^{1}H-NMR using 1,3,5-trimethoxybenzene as internal standard.

Synthesis of peptide conjugate **6**: the tetrapeptide was made on solid phase on a 0.1 mmol scale using the standard Fmoc-based amino acid protection strategy on H-Rink amide *ChemMatrix*® resin (0.49 mmol/g) using a mixture of HOBT/HBTU (1:1) as activating agent, DIEA as base, and DMF as solvent. Fmoc-Lysine was used protected as alloc (Fmoc-Lys(Alloc)-OH). After introducing this N-terminal lysine, Fmoc was cleaved by treatment with 20% piperidine in DMF (20 min). The resulting amino group was coupled to BTTAA using 2.0 eq. of this carboxylic acid (86. mg, 0.2 mmol), 2.0 eq. of HBTU and 2.0 eq. of HOBT (0.2 M solution in DMF) and 3.0 eq. of DIEA (0.2 M in DMF) for 60 min. Finally, the alloc group was removed, and the resulting amine coupled to the succinimidyl ester of fluorophore TAMRA (6-carboxytetramethylrhodamine *N*-succinimidyl ester), using 1.0 eq. of 6-TAMRA-NHS (52.8 mg, 0.1 mmol), and 3.0 eq. of DIEA (0.2 M in DMF) for 60 min.

The Alloc removal was performed by treating the resin-bound peptide for 20 min with a mixture of $Pd(PPh_3)_4$ (11.6 mg, 0.01 mmol, 10 mol%) and phenylsilane (248.0 µL, 2.0 mmol, 20 eq.) in CH_2Cl_2 (6.0 mL). The resin was then washed with CH_2Cl_2 three times, and the process was repeated. Finally, the resin was washed twice with a solution of sodium diethyldithiocarbamate in DMF.

The resulting resin-bound peptide was treated for 2 h with the following cleavage cocktail: 900 µL trifluoroacetic acid, 50 µL CH_2Cl_2, 25 µL H_2O and 25 µL triisopropylsilane (1 mL of cocktail / 40 mg resin). The resin was filtered, and the TFA filtrate was concentrated with a nitrogen current to an approximate volume of 1 mL, which was added to ice-cold diethyl ether (10 mL). After 10 min, the precipitate was centrifuged and washed again with 15 mL of ice-cold ether. The solid residue was dried under argon, dissolved in MeCN/water 1:1 and purified by semi-preparative reverse-phase HPLC, 3.5 mL/min, gradient 5 to 75% B over 20 min (A: H_2O 0.1% TFA, B: MeCN 0.1% TFA) on a semipreparative *Agilent Eclipse*–C18 (250 × 10 mm) reverse-phase column.

Cell culture experiments. Cell lines were cultured in DMEM containing 5 mM glutamine, penicillin (100 units mL–1) and streptomycin (100 units mL–1) (all from *Invitrogen*). Proliferating cell cultures were maintained in a humidified incubator at 37 °C and 5% CO_2 atmosphere. All incubations were performed in DMEM at 37 °C. Cells were seeded two days before treatment.

Representative procedure for the synthesis of 3a in living cells. Cells growing on glass coverslips were incubated with the copper complex (50 µM) for 50 min, washed twice with DMEM and incubated with substrates **1** and **2a** (100 µM) for 3 h. The samples were washed twice with fresh DMEM and the coverslips observed *in vivo* in a fluorescence microscope equipped with adequate filters. Identical conditions of gain and exposure were applied for all the digital pictures of the different samples.

Representative procedure for the synthesis of 3c in living cells, and monitoring mitochondria depolarization. Cells growing on glass coverslips were incubated with copper complex (25-50 μM) for 50 min, washed twice with DMEM and incubated with substrates **1** and **2c** (50-100 μM) for 3.5 h. Then TMRE (100 nM) was added and the cells were incubated for 10 min. The samples were washed twice with fresh DMEM and the coverslips observed in vivo in a fluorescence microscope equipped with adequate filters. Identical conditions of gain and exposure were applied for all the digital pictures of the different samples.

ICP analysis. For the ICP measurements, a total of 3×10^6 HeLa cells growing in six well plates were treated with 50 μM of $Cu(OAc)_2$ in DMEM for 50 min. Prior to digestion, the samples were thoroughly washed with fresh DMEM and then twice with PBS, to ensure removal of the external copper salts. The obtained fractions were digested in duplicate in HNO_3/H_2O_2 by microwave heating and analyzed.

Quantification studies. For the quantification of the copper catalyzed reaction of **1** and **2a** in HeLa cells, a total of 12 x 10^6 HeLa cells growing in 6 plates of 100 mm were incubated with catalyst $Cu(OAc)_2$ (50 μM) for 50 minutes followed by two washing steps with DMEM. Then, cells were incubated with substrates **1** (100 μM) and **2a** (100 μM) for 3 h or 5 h. Afterwards, the reaction media was collected for analysis in a 50 mL Falcon. Prior to extraction, cells were washed with 3 mL of DMEM, followed by two washing steps with 3 mL of PBS and the washings were also collected separately in 50 mL Falcons. Then the cell monolayer was treated with 1 mL of MeOH. After 5 min and pipetting up this solution was transferred to a 15 mL Falcon. Finally, we obtained 6 mL of methanolic extracts from the six plates employed. All the samples were lyophilized for 3 days and dissolved in MeCN (until reaching a theoretical concentration of 250 μM). For the quantification of the product, the obtained samples were centrifuged at 13500 rpm for 15 minutes and the supernatant was collected. In the case of the methanolic extract, it was diluted 1:4 using $MeCN/H_2O$ 6:4. However, in the case of the samples of the reaction media, first, second and third washings, no dilution was required.
Each sample was injected in a Bruker Elute coupled with *timsTOF* using a column *Zorbax Eclipse XDB*-C18 2.1 x 100 mm 1.8 μm and a flow rate of 0.4 mL/min at room temperature. For the solvent system, initial conditions 80% B (A: H_2O 0.1% TFA, B: MeCN 0.1% TFA) were used for 1 min and followed by a gradual change over 7 min to 100% B, followed by a gradual change over 12 secs to 80% B and maintained for 2 min.. Further details on the mass spectrometry results are in the Supplementary Note 13.

Viability assays. The toxicity was analyzed by MTT assay in HeLa cell line as follows: 100000 cells per well were seeded in 96-well plates 2 days before treatment with different concentrations of the catalysts, substrates or products. After appropriate time of incubation, medium containing Thiazolyl Blue Tetrazolium Bromide (Sigma) was added to a final concentration of 0.5 mg ml -1. Cells were then incubated for 4 h to allow the formation of formazan precipitates by metabolically active cells. A detergent solution of 10% SDS and 0.01 M HCl was then added and the plate was incubated overnight at room temperature to allow the solubilization of the precipitates. The quantity of formazan in each well (directly proportional to the number of viable cells) was measured by recording changes in absorbance at 570 nm in a microtiter plate reading spectrophotometer (*Tecan Infinite 200 PRO*).

Data availability statement

The authors declare that the data supporting the findings of this study are available within the article and its Supplementary Information files. Other data that support the findings of this study are available from the corresponding author upon request.

Acknowledgements

This work has received financial support from Spanish grants (PID2019-108624RB-I00, RTI2018-093813-J-I00 and ORFEO-CINQA network CTQ2016-81797-REDC), the Consellería de Cultura, Educación e Ordenación Universitaria (2015-CP082, ED431C-2017/19 and Centro Singular de Investigación de Galicia accreditation 2019-2022, ED431G 2019/03), the European Union (European Regional Development Fund-ERDF corresponding to the multiannual financial framework 2014-2020), and the European Research Council (Advanced Grant No. 340055). S.G. thanks the European Union (European Regional Development Fund, Interreg V-A POCTEP España-Portugal programme, 2iqbioneuro project) and M.T.G. thanks the financial support from the Agencia Estatal de Investigación (RTI2018-093813-J-I00). The authors thank R. Menaya-Vargas for excellent technical assistance, the use of RIAIDT-USC analytical facilities and especially M. Marcos for excellent and essential contributions to the LC-MS analysis.

Author contributions

Affiliations

Centro Singular de Investigación en Química Biolóxica e Materiais Moleculares (CIQUS) and Departamento de Química Orgánica, Universidade de Santiago de Compostela, Santiago de Compostela, 15782, Spain

Sara Gutiérrez, María Tomás-Gamasa & José L. Mascareñas

Contribution

S.G. performed the chemical synthesis, in vitro experiments and analyzed the data. S.G. and M.T.G. performed cell-based experiments and analyzed the data. J.L.M. came up with the concept. J.L.M. and M.T.G. guided the research, and all the authors conceived experiments, interpreted the results, and participated in writing the manuscript.

Corresponding author

Correspondence to María Tomás-Gamasa or José L. Mascareñas

Competing interests

The authors declare no competing interest.

REFERENCES

1. Martínez Cuesta, S., Rahman, S. A., Furnham, N. & Thornton, J. M. The Classification and evolution of enzyme function. *Biophys J.* **109**, 1082-1086 (2015).

2. Alberts, B. *et al. Molecular Biology of the Cell* (Garland Science; 6th edition, New York & Abingdon, UK, 2017).

3. Vornholt, T. *et al*.. Systematic engineering of artificial metalloenzymes for new-to-nature reactions. *Science Advances* **7**, eabe4208 (2021).

4. Bäckvall, J.-E., Diéguez, M. & Pamiès, O. *Artificial Metalloenzymes and MetalloDNAzymes in Catalysis: From Design to Applications* (Wiley-VCH Verlag GmbH & Co. KGaA, 2018).

5. Schwizer, F. *et al.*. Artificial metalloenzymes: Reaction scope and optimization strategies. *Chem. Rev.* **118**, 142-231 (2018).

6. Davis, H. J. & Ward, T. R. Artificial metalloenzymes: Challenges and opportunities. *ACS Cent. Sci.* **5**, 1120-1136 (2019).

7. Matsuo, T., Miyake, T. & Hirota, S. Recent developments on creation of artificial metalloenzymes. *Tetrahedron* Lett. **60**, 151226-151233 (2019).

8. Hyster, T. K. & Ward, T. R. Genetic optimization of metalloenzymes: Enhancing enzymes for non-natural reactions. *Angew. Chem. Int. Ed.* **55**, 7344-7357 (2016).

9. Liang, A. D., Serrano-Plana, J., Peterson, R. L. & Ward, T. R. Artificial metalloenzymes based on the Biotin–Streptavidin technology: enzymatic cascades and directed evolution. *Acc. Chem. Res.* **52**, 585-595 (2019).

10. Chordia, D., Narasimhan, S., Paioni, A. L., Baldus, M. & Roelfes, G. In vivo assembly of artificial metalloenzymes and application in whole-cell biocatalysis. *Angew. Chem. Int. Ed.* 2021, **8**, 5913-5920 (2021).

11. Maaskant, R-.V., Chordia, S. & Roelfes, G. Merging whole-cell biosynthesis of styrene and transition-metal catalyzed derivatization reactions. *ChemCatChem.* DOI: 10.1002/cctc.202001896 (2021).

12. Jeschek, M., Panke, S. & Ward, T. R. Artificial metalloenzymes on the verge of new-to-nature metabolism. *Trends Biotechnol.* **36**, 60-72 (2018).

13. Tanaka K. & Vong, K. Unlocking the therapeutic potential of artificial metalloenzymes. *Proc. Jpn Acad. Ser. B Phys. Biol. Sci.* **96**, 79-94 (2020).

14. Destito, P., Vidal, C., López, F. & Mascareñas, J. L. Transition metal-promoted reactions in aqueous media and biological settings. *Chem. Eur. J.* DOI: 10.1002/chem.20200392 (2020).

15. Liu, Y. & Bai, Y. Design and engineering of metal catalysts for bio-orthogonal catalysis in living systems. *ACS Appl. Bio Mater.* **3**, 4717-4746 (2020).

16. Martínez-Calvo, M. & Mascareñas, J. L. Organometallic catalysis in biological media and living settings. *Coord. Chem. Rev.* **359**, 57-79 (2018).

17. Ngo, A. H., Bose, S. & Do, L. H. Intracellular chemistry: integrating molecular inorganic catalysts with living systems. *Chem. Eur. J.* **24**, 10584-10594 (2018).

18. Bai, Y., Chen, J. & Zimmerman, S. C. Designed transition metal catalysts for intracellular organic synthesis. *Chem. Soc. Rev.* **47**, 1811-1821 (2018).

19. Soldevilla-Barreda, J. J. & Metzler-Nolte, N. Intracellular catalysis with selected metal complexes and metallic nanoparticles: advances toward the development of catalytic metallodrugs. *Chem. Rev.* **119**, 829-869 (2019).

20. Streu, C. & Meggers, E. Ruthenium-induced allylcarbamate cleavage in living cells. *Angew. Chem. Int. Ed.* **45**, 5645-5648 (2016).

21. Völker, T., Dempwolff, F., Graumann, P. L. & Meggers, E. Progress towards bioorthogonal catalysis with organometallic compounds. *Angew. Chem. Int. Ed.* ***5*3**, 10536-10540 (2014).

22. Sánchez, M. I., Penas, C., Vázquez, M. E. & Mascareñas, J. L. Metal-catalyzed uncaging of DNA-binding agents in living cells. *Chem. Sci.* **5**, 1901-1907 (2014).

23. Tonga, G. Y. *et al.* Supramolecular regulation of bioorthogonal catalysis in cells using nanoparticle-embedded transition metal catalysts. *Nat. Chem.* **7**, 597-603 (2015).

24. Tomás-Gamasa, M., Martínez-Calvo, M., Couceiro, J. R. & Mascareñas, J. L. Transition metal catalysis in the mitochondria of living cells. *Nat. Commun.* **7**, 12538-12547 (2016).

25. Martínez-Calvo, M. *et al.* Intracellular deprotection reactions mediated by palladium complexes equipped with designed phosphine ligands. *ACS Catal.* **8**, 6055-6061 (2018).

26. Stenton, B. J., Oliveira, B. L., Matos, M. J., Sinatra, L. & Bernardes, G. J. L. A thioether-directed palladium-cleavable linker for targeted bioorthogonal drug decaging. *Chem. Sci*. **9**, 4185-4189. (2018).

27. Martínez, R. *et al.* Core-shell palladium/MOF platforms as diffusion-controlled nanoreactors in living cells and tissue models. *Cell. Rep. Phys. Sci.* **1**, 100076 (2020).

28. Vidal, C., Tomás-Gamasa, M., Destito, P., López, F. & Mascareñas, J. L. Concurrent and orthogonal gold(I) and ruthenium(II) catalysis inside living cells. *Nat. Commun.* **9**, 1913 (2018).

29. Miller, M. A. *et al.* Nano-palladium is a cellular catalyst for *in vivo* chemistry. *Nat. Commun*. **8**, 15906-15918 (2017).

30. Destito, P. *et al* Hollow nanoreactors for Pd-catalyzed Suzuki-Miyaura couplings and also o-propargyl cleavage reactions in relevant aqueous media. *Chem. Sci.* **10**, 2598-2603 (2019).

31. Yusop, R. M., Unciti-Broceta, A., Johansson, E. M. V., Sánchez-Martín, R. M. & Bradley, M. Palladium-mediated intracellular chemistry. *Nat. Chem.* **3**, 2399-243 (2011).

32. Toussaint, S. N. W., Calkins, R. T., Lee, S., & Michel, B. W. Olefin metathesis-based fluorescent probes for the selective detection of ethylene in live cells. *J. Am. Chem. Soc.* **140**, 13151-13155 (2018).

33. Wang, F., Zhang, Y., Du, Z., Ren, J. & Qu, X. Designed heterogeneous palladium catalysts for reversible light-controlled bioorthogonal catalysis in living cells. *Nat. Commun.* **9**, 1209 (2018).

34. Destito, P., Couceiro, J. R., Ferreira, H., López, F. & Mascareñas, J. L. Ruthenium-catalyzed azide-thioalkyne cycloadditions in aqueous media: a mild, orthogonal, and biocompatible chemical ligation. *Angew. Chem. Int. Ed.* **56**, 10766-10770 (2017).

35. Miguel-Ávila, J., Tomás-Gamasa, M. & Mascareñas, J. L. Intracellular ruthenium-promoted (2+2+2) cycloadditions. *Angew. Chem. Int. Ed.* **59**, 17628-17633 (2020).

36. Miguel-Ávila, J., Tomás-Gamasa, M., Olmos, A., Pérez, P. J. &. Mascareñas, J. L. Discrete Cu(I) complexes for azide–alkyne annulations of small molecules inside mammalian cells. *Chem. Sci.* **9**, 1947-1952 (2018).

37. Li, S., Wang, L. *et al.* Copper-catalyzed click reaction on/in live cells. *Chem. Sci.* **8**, 2107-2114 (2017).

38. Bai, Y. *et al.* Highly efficient single-chain metal–organic nanoparticle catalyst for alkyne–azide "click" reactions in water and in cells. *J. Am. Chem. Soc.* **138**, 11077-10080 (2016).

39. Zaragoza Dörwald, F. *Metal Carbenes in Organic Synthesis* (WILEY-VCH Verlag GmbH, 1999).

40. Dai, S.-Y. & Yang, D. A visible and near-infrared light activatable diazocoumarin probe for fluorogenic protein labeling in living cells. *J. Am. Chem. Soc.* **142**, 17156-17166 (2020).

41. Antos, J. M. & Francis, M. B. Selective tryptophan modification with rhodium carbenoids in aqueous solution. *J. Am. Chem. Soc.* **126**, 10256-10257 (2004).

42. Antos, J. M., McFarland, J. M., Iavarone, A. T. & Francis, M. B. Chemoselective tryptophan labeling with rhodium carbenoids at mild pH. *J. Am. Chem. Soc.* **131**, 6301-6308 (2009).

43. Popp, B. V. & Ball, Z. T. Structure-selective modification of aromatic side chains with dirhodium metallopeptide catalysts. *J. Am. Chem. Soc.* **132**, 6660-6662 (2010).

44. Popp, B. V. & Ball, Z. T. Proximity-driven metallopeptide catalysis: Remarkable side-chain scope enables modification of the Fos bZip domain. *Chem. Sci.* **2**, 690-695 (2011).

45. Chen, Z. *et al.* Catalytic protein modification with dirhodium metallopeptides: specificity in designed and natural systems. *J. Am. Chem. Soc.* **134**, 10138-10145 (2012).

46. Vohidov, F., Coughlin, J. M. & Ball, Z. T. Rhodium(II) metallopeptide catalyst design enables fine control in selective functionalization of natural SH3 Domains. *Angew. Chem. Int. Ed*. **54**, 4587-4591 (2015).

47. Ohata, J. & Ball, Z. T. A hexa-rhodium metallopeptide catalyst for site-specific functionalization of natural antibodies. *J. Am. Chem. Soc.* **139**, 12617-12622 (2017).

48. Tishinov, K., Schmidt, K., Häussinger, D. & Gillingham, D. G. Structure-selective catalytic alkylation of DNA and RNA. *Angew. Chem. Int. Ed.* **51**, 12000-12004 (2012).

49. Tishinov, K., Fei, N. & Gillingham, D. Cu(I)-catalysed N–H insertion in water: a new tool for chemical biology. *Chem. Sci.* **4**, 4401-4406 (2013).

50. Key, H. M., Dydio, P., Clark, D. S. & Hartwig, J. F. Abiological catalysis by artificial haem proteins containing noble metals in place of iron. *Nature* **534**, 534-537 (2016).

52. Dydio, P. *et al.* An artificial metalloenzyme with the kinetics of native enzymes. Science **354**, 102-106 (2016).

53. Zhang, R. K. *et al.* Enzymatic assembly of carbon–carbon bonds via iron-catalysed sp^3 C–H functionalization. *Nature*, **546**, 67-72 (2019).

54. Coelho, P. S. *et al.* A serine-substituted p450 catalyzes highly efficient carbene transfer to olefins in vivo. *Nat. Chem. Biol.* **9**, 485-487 (2013)

55. Kan, S. B. J., Lewis, R. D., Chen, K. & Arnold, F. H. Directed evolution of cytochrome c for carbon–silicon bond formation: Bringing silicon to life. *Science* **354**, 1048-1051 (2016).

56. Lewis, R. D. *et al.* Catalytic iron-carbene intermediate revealed in a cytochrome *c* carbene transferase. *Proc Natl Acad Sci U S A* 115, 7308-7313 (2018).

57. Kan, S. B. J., Huang, X., Gumulya, Y., Chen, K. & Arnold, F. H. Genetically programmed chiral organoborane synthesis. *Nature* **552**, 132-136 (2017).

58. Chandgude, A. L., Ren, X. & Fasan, R. Stereodivergent intramolecular cyclopropanation enabled by engineered carbene transferases. *J. Am. Chem. Soc.* **141**, 9145-9150 (2019)

59. Sreenilayam, G. & Fasan, R. Myoglobin-catalyzed intermolecular carbene N–H insertion with arylamine substrates. *Chem. Commun*. **51**, 1532-1534 (2015).

60. Arnold, F. H. Directed Evolution: Bringing new chemistry to life. *Angew. Chem. Int Ed.* **57**, 4143-4148 (2018).

61. Wallace, S. & Balskus, E. P. Interfacing microbial styrene production with a biocompatible cyclopropanation reaction. *Angew. Chem.* Int. Ed. **54**, 7106-7109 (2015).

62. Pandit, R. M., Kim, S. H. & Lee, Y. R. Iron-catalyzed annulation of 1,2-diamines and diazodicarbonyls for diverse and polyfunctionalized quinoxalines, pyrazines, and benzoquinoxalines in water. *Adv. Synth. Catal.* **358**, 3586-3599 (2016).

63. Uttamapinant, C. *et al.* Fast, cell-compatible click chemistry with copper-chelating azides for biomolecular labeling. *Angew. Chem. Int. Ed.* **51**, 5852-5856 (2012).

64. Bevilacqua, V. *et al.* Copper-chelating azides for efficient click conjugation reactions in complex media. *Angew. Chem. Int. Ed.* **53**, 5872-5876 (2014).

65. Ramakrishna K. & Sivasankar, C. Iridium catalyzed acceptor/acceptor carbene insertion into N–H bonds in water. *Org. Biomol. Chem.* **15**, 2392-2396 (2017).

66. Van de L'Isle, M.O. N., Ortega-Liebana, M. C. & Unciti-Broceta, A. Transition metal catalysts for the bioorthogonal synthesis of bioactive agents. *Curr. Opin. Chem. Biol.* **61**, 32-42 (2021).

67. Vidal, C., Tomás-Gamasa, M., Gutiérrez-González, A. & Mascareñas, J. L. Ruthenium-catalyzed redox isomerizations inside living cells. *J. Am. Chem. Soc*. **141**, 5125-5129 (2019).

68. Sabatino, V., Rebelein, J. G. & Ward, T. R. "Close-to-Release": spontaneous bioorthogonal uncaging resulting from ring-closing metathesis. *J. Am. Chem. Soc.* **141**, 17048-17052 (2019).

69. Huang, J. S. *et al.* Nanocopper-doped cross-linked lipoic acid nanoparticles for morphology-dependent intracellular catalysis. *ACS Catal.* **8**, 5941-5946 (2018).

70. Wang, F. M. *et al.* A biocompatible heterogeneous MOF-Cu catalyst for in vivo drug synthesis in targeted subcellular organelles. *Angew. Chem. Int. Ed.* **58**, 6987-6992 (2019).

71. Levitzki, A. & Mishani, E. Tyrphostins and other tyrosine kinase inhibitors. *Annu. Rev. Biochem.* **75**, 93-109 (2006).

72. Park, S. J. *et al.* A receptor tyrosine kinase inhibitor, Tyrphostin A9 induces cancer cell death through Drp1 dependent mitochondria fragmentation. *Biochem. Biophys. Res. Comm.* **408**, 465-470 (2011).

73. Gazit, A. *et al.* Tyrphostins. 5. Potent inhibitors of platelet-derived growth factor receptor tyrosine kinase: structure-activity relationships in quinoxalines, quinolines, and indole Tyrphostins. *J. Med. Chem.* **39**, 2170 (1996).

74. Chalmers, S. *et al.* Selective uncoupling of individual mitochondria within a cell using a mitochondria-targeted photoactivated protonophore. *J. Am. Chem. Soc.* **134**, 2, 758-761 (2012).

75. Learte-Aymamí, S., Vidal, C., Gutiérrez-González, A. & Mascareñas. J. L. Intracellular reactions promoted by bis(histidine) miniproteins stapled using palladium(II) complexes. *Angew. Chem. Int. Ed.* **59**, 9149-9154 (2020).

Table of content graphic (TOC)

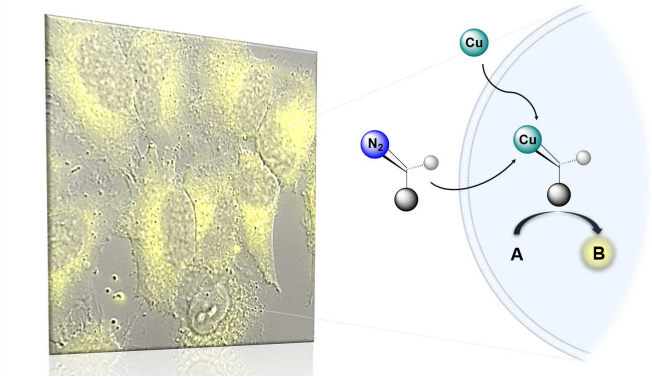

Figures

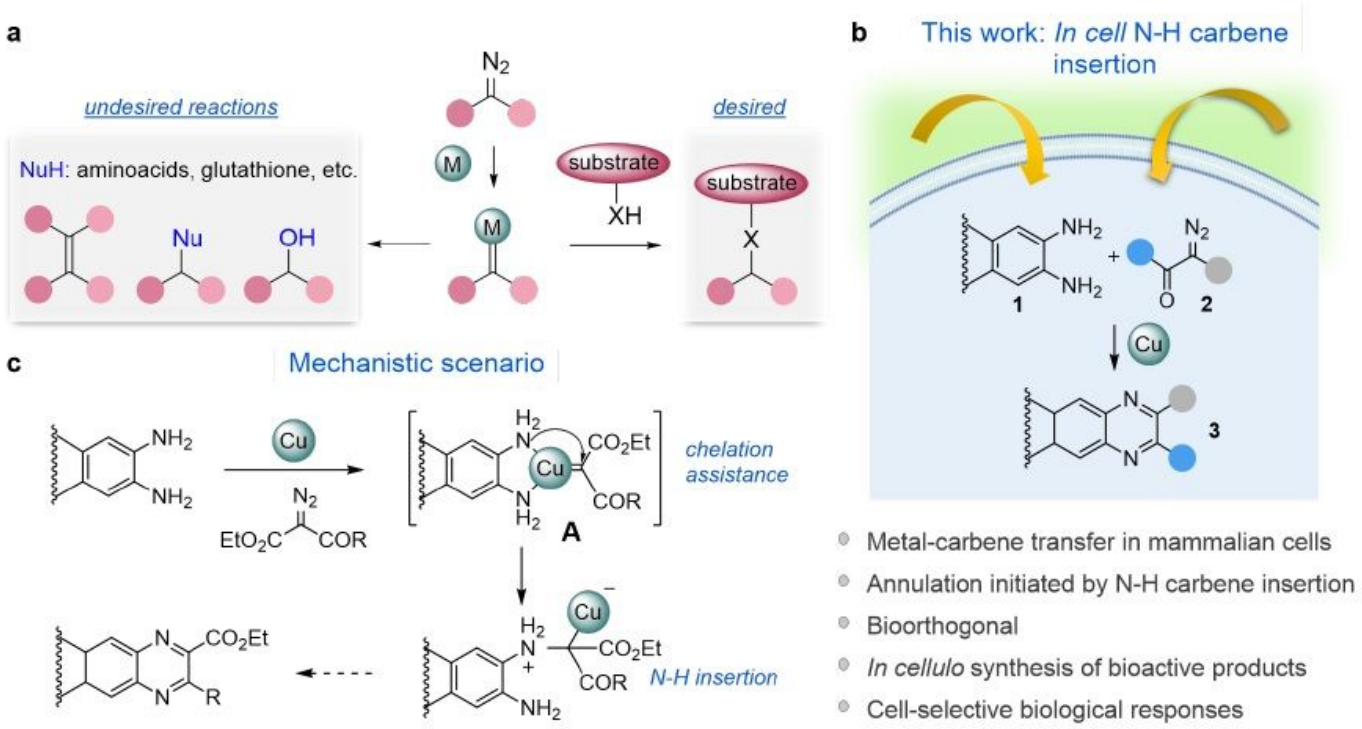

Figure 1

Metal N-H carbene insertions in biological settings. a, Orthogonality challenges in metalmediated carbene transfer transformations in aqueous/biological media. b, Copper-promoted annulation initiated by an N-H carbene insertion within biological and/or cellular environments. c, Mechanistic outline: The copper carbene sticks to the diamine owing to the bidentate coordination. This might favor the N-H insertion, which is followed by an intramolecular condensation and oxidative aromatization.

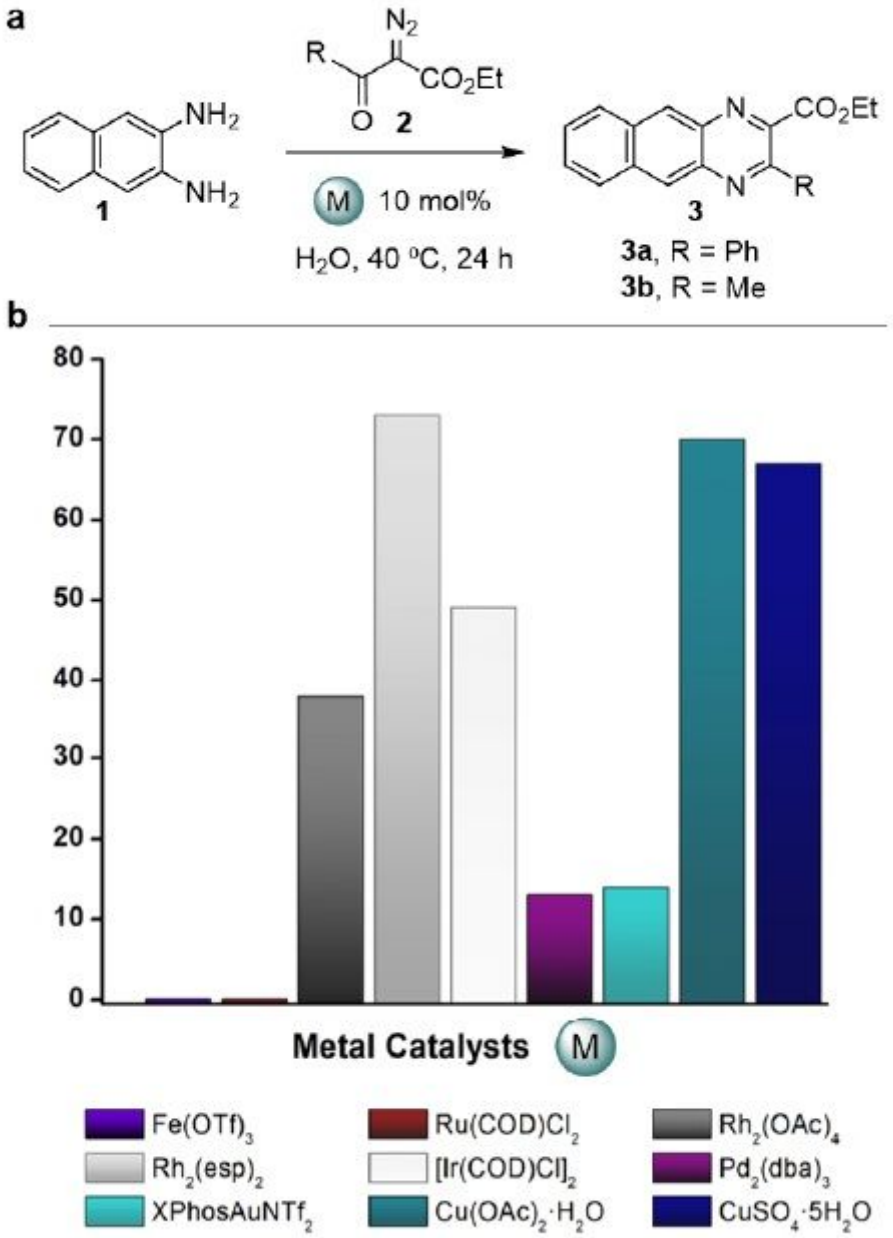

Figure 2

Metal-catalyzed assembly of quinoxalines in water. a, Annulation reaction. b, Screening of different transition metal catalysts. a Reaction conditions: 1 equiv. 1 and 2, in H2O (100 mM), in presence of 10 mol% catalyst, and heating of the resulting heterogeneous mixture at 40 °C for 24 h. Yield calculated by 1H-NMR using 1,3,5-trimethoxybenzene as internal standard.

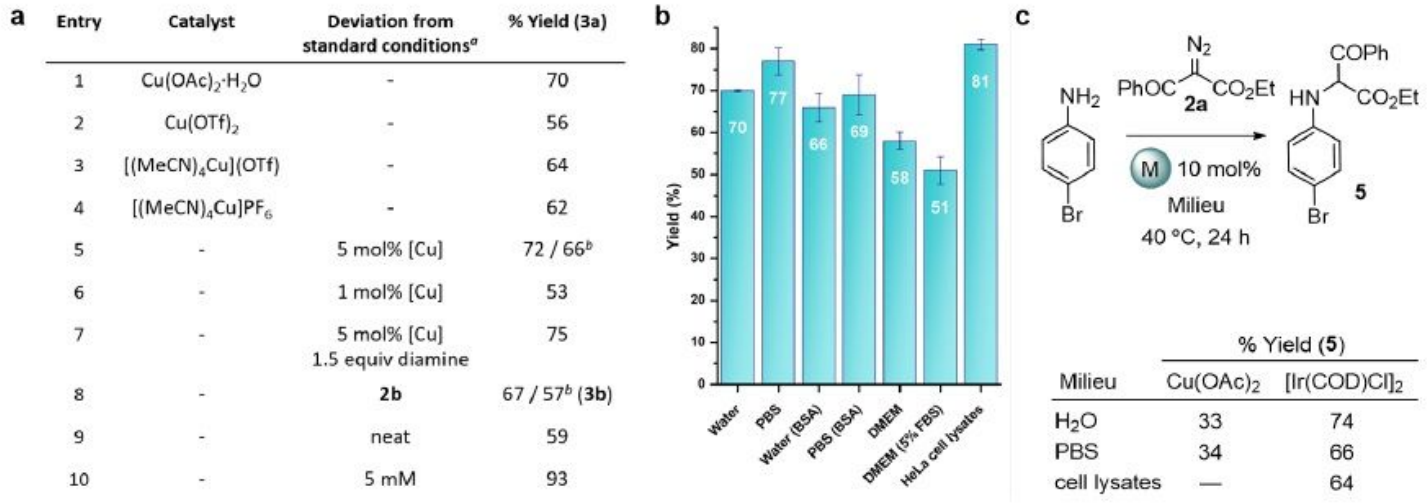

Figure 3

Copper-carbene mediated synthesis of quinoxalines 3. a, Further optimization of the reaction between 1 and 2a or 2b. b, Efficiency in presence of biological buffers. BSA 5 mg/mL; Cell lysates 4 mg/mL (the values are average of three experiments, and error bars correspond to standard deviations). c, Monoaminations by N-H insertion. a Reaction conditions: H2O as solvent, 100 mM, 10 mol% catalyst, 40 °C, 24 h; [Cu] = Cu(OAc)2. Yield calculated by 1H-NMR using 1,3,5-trimethoxybenzene as internal standard. b Isolated yield.

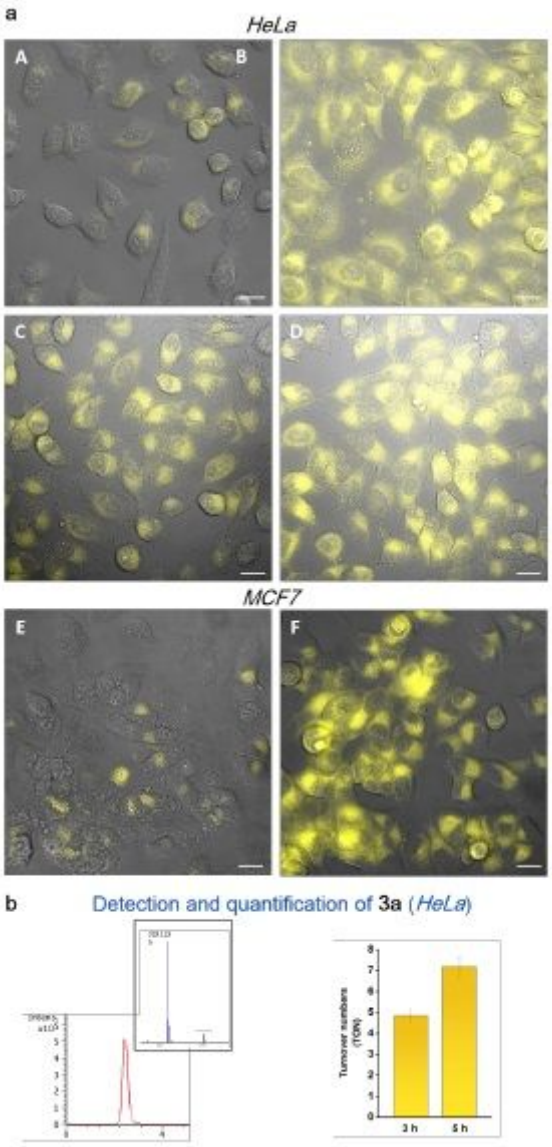

Figure 4

Synthesis of 3a inside live HeLa cells. a, Fluorescence micrographies (brightfield) of HeLa (A-D) and MCF7 cells (E,F) after incubation with: 1 and 2a (A, E); 3a (B) or Cu(OAc)2, washing, and treatment with 1 and 2a for 1.5 h (C) or for 3 h (D,F). Reactions conditions: Cells were pretreated with 50 μM of Cu(OAc)2 (stock solution in H2O) for 50 min, washed twice with DMEM, and incubated with 100 μM of substrates 1 and 2a (stock solutions in DMEM) for the indicated time. b, Detection and quantification of 3a in HeLa cells. Left: Extracted ion chromatogram of the product (3a) generated intracellularly (methanolic extract); Right: Quantification of turnover numbers (average of three experiments), considering the product present in the cell media and washes (2xDMEM, 1xPBS) and in the methanolic cellular extracts (over 75% of the total). Scale bar: 20 μm. lexc = 385 nm, lem > 520 nm.

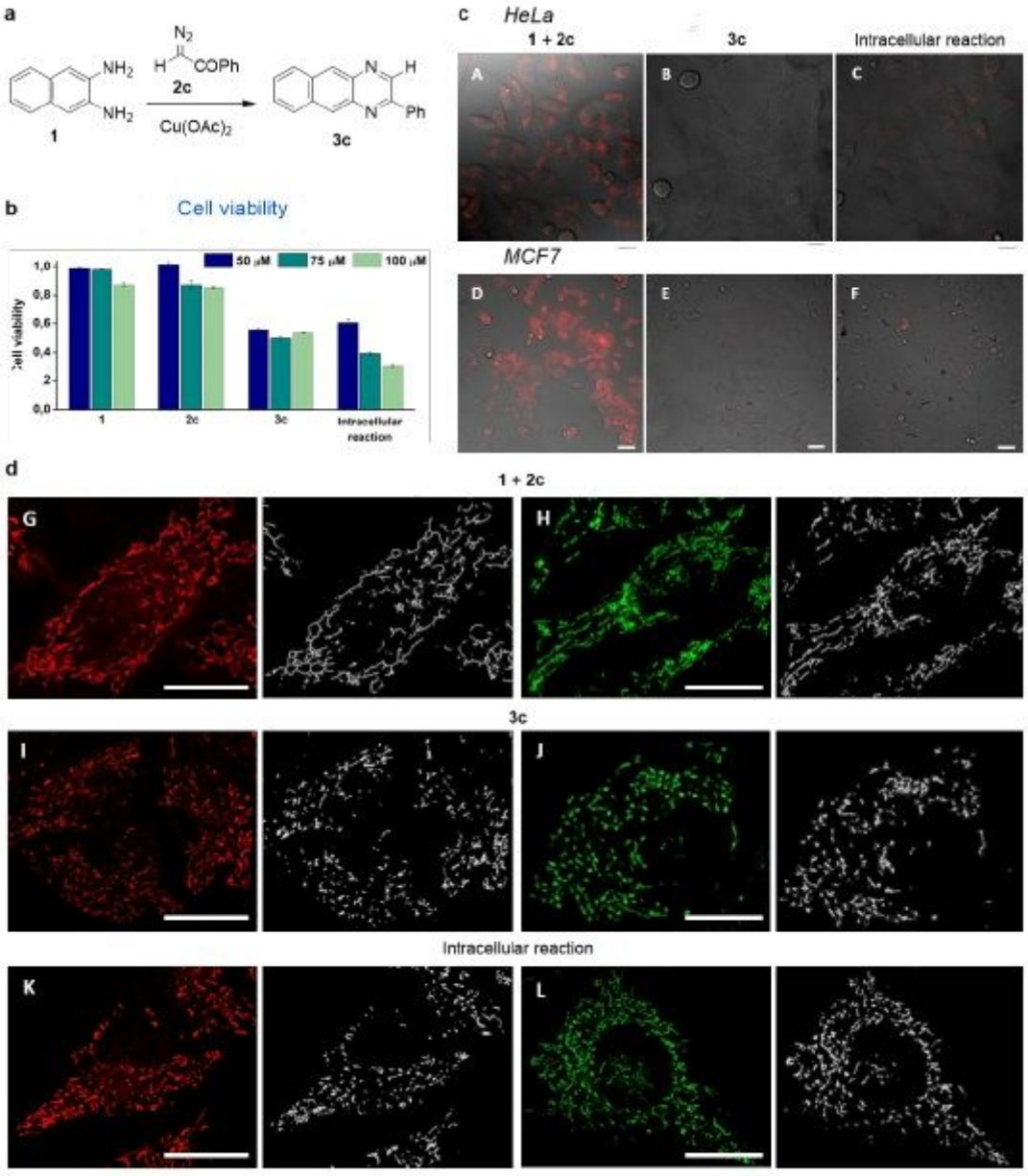

Figure 5

Intracellular generation of 3c. a, Synthesis of 3c. b, Cytotoxicity studies. HeLa cells were mixed with either 1 and 2c, or 3c (50-100 μM) for 12 h; for the intracellular reaction cells were incubated with Cu(OAc)2 (25-50 μM) for 50 min, washed twice with DMEM and treated with substrates 1 and 2c (50-100 μM) for 12 h. c, Mitochondrial depolarization. Fluorescence micrographies using TMRE as marker: HeLa (A-C), and MCF7 cells (D-F) (brightfield) after incubation with: 1 and 2c (A,D); 3c (B,E); Cu(OAc)2, washing, and treatment with 1 and 2c (C,F) for 3.5 h. d, Mitochondrial fragmentation. Fluorescence micrographies of HeLa cells (brightfield) using TMRE (G,I,K) or MitoTracker Green (H,J,L) as marker, after incubation with: 1 and 2c (G,H); 3c (I,J) or Cu(OAc)2, washing and treatment with 1 and 2c for 8 h (K) or 2 h (L); in white, mitochondrial staining from each image displayed as a skeleton network using the ImageJ skeleton filter, which allows a better visualization of the fragmentation. Reaction conditions: Cells were mixed with 1 and 2c, or 3c. For the intracellular reaction cells were incubated with Cu(OAc)2 (50 μM) for 50 min,

washed twice with DMEM and treated with substrates 1 and 2c (100 µM) and incubated with TMRE or MitoTracker Green (100 nM) for 10 min. Scale bar: 20 µm (15 µm in section c). lexc = 550 nm, lem = 570-590 nm for panels A-K; lexc = 470 nm, lem = 490-580 nm for panels H-L.

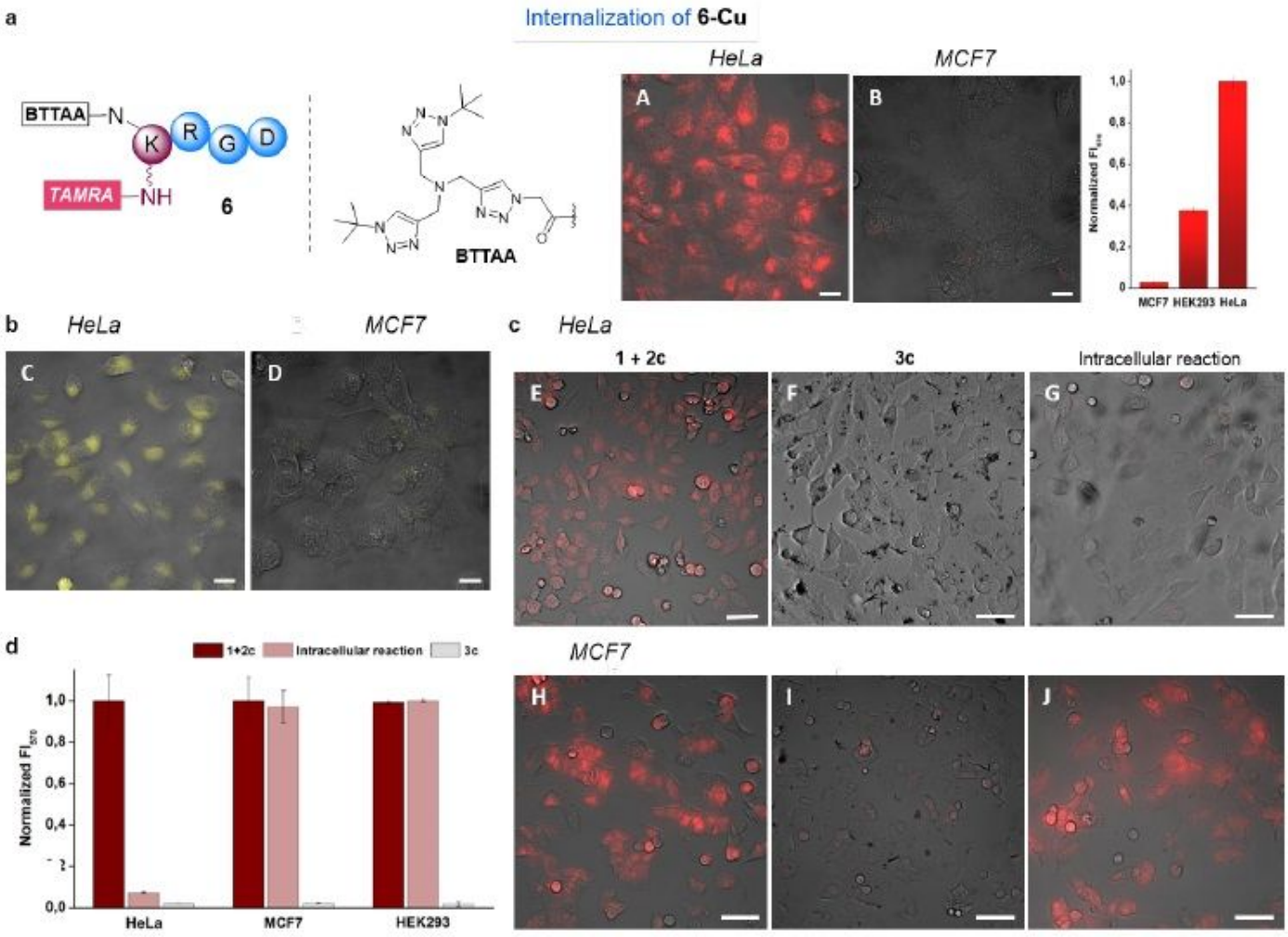

Figure 6

Selective cellular targeting using a RGD copper-containing peptide (6-Cu). a, Structure of the RGD containing ligand in 6-Cu; Comparison of internalization of 6-Cu. Fluorescence micrographies of HeLa (A) and MCF7 cells (B) (brightfield) and CTCF measurements in HeLa, MCF7 and HEK293 cells. Conditions: cells were incubated with 15 µM of 6-Cu for 1.5 h. b, Fluorescence micrographies of HeLa (C) and MCF7 cells (D) (brightfield) after incubation with 6-Cu, washing, and treatment with 1 and 2a for 3.5 h. Scale bar: 20 µm. c, Cell-selective mitochondrial depolarization: Fluorescence micrographies of HeLa (E-G) and MCF7 cells (H-J) (brightfield) after incubation with: 1 and 2c (E,H), product 3c (F,I), or 6-Cu, washing, and treatment with 1 and 2c for 3.5 h (G, J). d, Bar graphic including CTCF measurements of mitochondrial depolarization in HeLa, MCF7 and HEK293 cells. Reaction conditions: cells were mixed with 6-Cu (15 µM) for 1.5 h, washed twice with DMEM and treated with 1 and 2a, or 1 and 2c (100 µM) for 3.5 h followed by

TMRE (100 nM) for 10 min. Scale bar: 100 μm. lexc = 550 nm, lem = 570-590 nm for panels (A,B,E-J); lexc = 385 nm, lem > 520 nm for panels (C,D).

Supplementary Files

This is a list of supplementary files associated with this preprint. Click to download.

- supplementaryinformation.pdf